Influence of salinity on the unconfined compressive strength of sands at different freezing temperatures

Author 1

- Nico Molls, M.Sc.
- Chair of Geotechnical Engineering and Institute of Geomechanics and Underground Technology, RWTH Aachen University, Im Süsterfeld 9, 52072 Aachen, Germany.
- ORCID number: 0009-0008-4480-4795
- e-mail: molls@gut.rwth-aachen.de
- phone: +49 241 80 2525 8

Author 2

- Raul Fuentes, Univ.-Prof. Dr.
- Chair of Geotechnical Engineering and Institute of Geomechanics and Underground Technology, RWTH Aachen University, Im Süsterfeld 9, 52072 Aachen, Germany
- ORCID number: 0000-0001-8617-7381
- e-mail: raul.fuentes@gut.rwth-aachen.de
- phone: +49 241 80 2524 7

Abstract

Salinity modifies the freezing behaviour of soils and can strongly affect the strength of frozen ground, yet the coupled relationships between phase behaviour, unfrozen water and mechanical response remain insufficiently documented. This study investigates the influence of NaCl on the freezing behaviour and unconfined compressive strength of fully saturated, narrow-graded sand. Freezing curves were recorded and interpreted together with nuclear magnetic resonance measurements of unfrozen water content and unconfined compression tests at -10 °C and -25 °C, representing conditions above and below the eutectic temperature of the NaCl-H_2O system.

Increasing NaCl concentration lowered both the supercooling temperature and the freezing temperature. At -10 °C, the unfrozen water content increased almost linearly with salinity, and even a small NaCl addition caused a disproportionate loss of strength: 0.5% NaCl reduced peak strength to about one quarter of the salt-free reference value. At -25 °C, the freezing curves exhibited a second plateau in saline specimens, consistent with eutectic solidification of residual brine. Under these conditions, the strength response differed qualitatively from that at -10 °C, showing a local plateau or partial recovery at low salinity before decreasing again at higher NaCl contents. Comparison between measured unfrozen water contents and a corrected lever-rule estimate showed good agreement up to about 5.0% NaCl for -10 °C.

The results provide a controlled thermo-mechanical dataset linking phase behaviour, unfrozen water and strength in saline frozen sand. The results show that salinity must be treated as a primary design variable in frozen ground. Above the eutectic, even low NaCl contents can severely reduce strength, whereas below the eutectic the phase assemblage and mechanical response change fundamentally, producing a non-monotonic strength trend that requires further microstructural investigation.

Keywords

Frozen soils, Uniaxial compression tests, Sand, Salt, Sodium Chloride, NMR, SFCC, UWC

1 Introduction

Salinity modifies the freezing behaviour of soils for example, by depressing the equilibrium freezing temperature, changing ice nucleation and supercooling behaviour, and increasing the amount of unfrozen pore liquid at sub-zero temperatures (Loomis, 1896; Atkins, 1996; Haghighi, Chapoy and Tohidi, 2008; Watanabe and Mizoguchi, 2002; Zhou et al., 2018; Wan, Liu and Qiu, 2021; Wang et al., 2023; Wan et al., 2024; Ying et al., 2025). These effects are important in both artificial ground freezing (AGF) and permafrost engineering, where salinity can influence not only phase change but also freezing rates, thermal conductivity and coupled heat–water–ice processes (McKenzie, Voss and Siegel, 2007; Jessberger and Jagow-Klaff, 2001; Ju et al., 2023). In AGF, saline groundwater can delay freezing and reduce the effectiveness of frozen support, as reported for cross-passage construction beneath the Suez Canal, where groundwater salinity required lower refrigeration temperatures than anticipated (Orth et al., 2021; Rizos et al., 2022). In cold regions, naturally saline soils and saline pore water can also alter freeze-thaw behaviour, unfrozen water retention and the resulting hydro-mechanical response of the ground (Wan et al., 2015; Luo et al., 2023).

Although the thermal effects of salinity are well established, the corresponding mechanical implications are less clearly quantified. The strength of frozen soil depends strongly on the amount, continuity and bonding role of the ice phase. Any process that retains liquid brine within the pore space at sub-zero temperatures can therefore reduce load-bearing capacity (Watanabe and Mizoguchi, 2002; Hivon and Sego, 1995). Previous studies have shown that increasing salinity reduces the strength of frozen soils (Hivon and Sego, 1995) and alters the freezing behaviour of coarse-grained sands by promoting the retention of highly saline unfrozen water within the pore structure (Arenson and Sego, 2004; Arenson and Sego, 2006). At the same time, thermodynamic studies have shown that the NaCl-H_2O system is governed by a eutectic point at -21.15 °C, below which the remaining brine solidifies in a second freezing stage (Journaux et al., 2023).

For engineering practice, this distinction is important. Above the eutectic temperature, part of the pore fluid remains liquid, so the frozen soil skeleton is weakened by unfrozen brine. Below the eutectic, the residual brine solidifies and the phase assemblage changes fundamentally. However, comparatively few experimental studies have brought these aspects together in one controlled programme by combining cooling curves, direct measurements of unfrozen water and mechanical strength data for the same saline sand system. As a result, the link between phase behaviour, unfrozen water and strength remains insufficiently documented, particularly across temperatures above and below the eutectic. Previous studies have separately examined salinity effects on freezing behaviour, unfrozen water retention and frozen-soil strength. However, comparatively few datasets combine freezing curves, direct unfrozen-water measurements and mechanical strength tests for the same controlled saline sand system, particularly across temperatures deliberately selected above and below the NaCl–H_2O eutectic. This limits the ability to link phase state directly to mechanical behaviour.

The present study addresses this issue using a narrow-graded, fully saturated sand and NaCl solutions of controlled concentration. A coarse-grained material was selected to minimise pore-size-controlled freezing effects and thereby isolate salinity-driven behaviour more clearly (Watanabe and Mizoguchi, 2002; Xiao, Lai and Zhang, 2018). Freezing curves were recorded during cooling, unconfined compression tests were performed after freezing, and unfrozen water contents were measured by nuclear magnetic resonance. Two test temperatures were selected: -10 °C, at which NaCl brine remains partly liquid, and -25 °C, which lies below the eutectic temperature of the NaCl-H_2O system (Journaux et al., 2023).

The objectives of this paper are threefold. First, it aims to quantify how NaCl concentration affects the freezing behaviour of saturated sand. Second, it examines how these changes influence unconfined compressive strength at temperatures above and below the eutectic. Third, it interprets the coupled thermal and mechanical response using the NaCl- H_2O phase diagram together with measured unfrozen water contents. The results show that even small

NaCl additions can cause a disproportionate loss of strength at -10 °C, whereas cooling below the eutectic introduces a second freezing stage associated with residual brine solidification and a qualitatively different strength response, where a local plateau or partial recovery in strength is observed at low salinity before strength decreases again at higher NaCl contents. The main contribution of the study is therefore a controlled thermo-mechanical dataset that directly links phase behaviour, unfrozen water and strength in saline frozen sand, with direct relevance to the assessment and design of artificial ground freezing works and saline frozen ground.

2 Thermodynamic background and research framework

2.1 Freezing of the NaCl-H_2O system

The freezing behaviour of saline pore water is governed by the phase relations of the NaCl-H_2O system. When NaCl is dissolved in water, the chemical potential of the liquid phase is reduced and the equilibrium freezing temperature decreases accordingly (Atkins, 1996; Haghighi, Chapoy and Tohidi, 2008). In a cooling saline system, ice does not initially form as a salt-bearing solid. Instead, relatively pure ice crystallises first, while the remaining liquid becomes progressively enriched in salt as freezing proceeds (Banin and Anderson, 1974). As a result, the liquid phase persists over a temperature range below 0 °C, rather than freezing completely at a single temperature.

For the NaCl-H_2O system at atmospheric pressure, this process continues until the eutectic state is reached. The eutectic temperature is approximately -21.15 °C and corresponds to a brine composition of about 23.3% NaCl by mass, at which the remaining liquid solidifies as a mixed solid assemblage rather than as pure ice alone (Atkins, 1996; Journaux et al., 2023). Above the eutectic, the relevant phase assemblage is therefore ice plus brine. Below the eutectic, the residual liquid phase disappears and the solid phase assemblage changes fundamentally. For the purposes of the present study, this distinction is central because specimens tested at -10 °C are expected to retain saline unfrozen water, whereas specimens tested at -25 °C are expected to have passed through eutectic solidification. Figure **1** shows

the NaCl-H_2O phase diagram and identifies the two test temperatures used in the experimental programme.

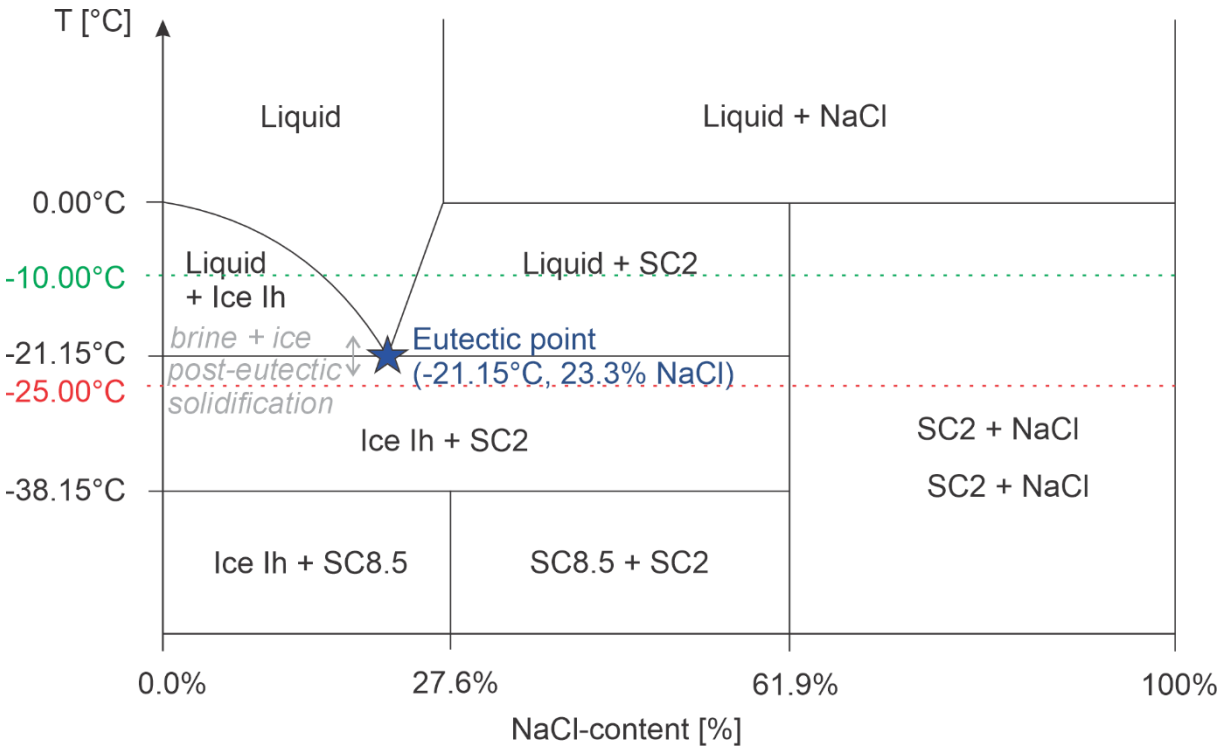

Fig. 1. NaCl-H_2O phase diagram at atmospheric pressure, showing the eutectic point and the two test temperatures used in the present study. At -10 °C, the specimens are expected to contain ice and unfrozen brine, whereas at -25 °C the cooling path lies below the eutectic temperature, so residual brine is expected to solidify in a second freezing stage (after Journaux et al., 2023).

In soils, phase change is additionally influenced by pore-scale processes. Capillary effects, interfacial forces, pore geometry and interfacial water all depress the freezing temperature relative to bulk water, so that part of the pore water remains unfrozen even in the absence of dissolved salts (Anderson and Tice, 1972; Anderson and Tice, 1973; Watanabe and Mizoguchi, 2002). When solutes are present, this pore-scale unfrozen water is supplemented by solute-induced freezing point depression, which increases the amount of liquid retained at a given sub-zero temperature (Watanabe and Mizoguchi, 2002). Recent soil-freezing-characteristic-curve models further emphasise that salt exclusion and dynamic water redistribution must be considered when interpreting liquid-water retention during freezing (Amankwah et al., 2021; Li, Li and Liu, 2024). In the present work, a narrow-graded coarse

sand was selected to reduce the influence of fine-pore freezing effects and to allow the influence of salinity to be interpreted more directly.

2.2 Unfrozen water and expected strength implications

The amount of unfrozen water is a key state variable for frozen soil because it links phase behaviour to engineering response. Measurements on porous media saturated with saline solutions have shown that the unfrozen water content increases with solute concentration and decreases with falling temperature (Watanabe and Mizoguchi, 2002). In saline soils, freezing therefore does not depend on temperature alone, but on the combined effects of temperature, pore structure and salt concentration. This is particularly important above the eutectic temperature, where a concentrated brine phase may remain in the pore space even when a substantial ice fraction has already formed.

From a mechanical perspective, frozen-soil strength depends strongly on the continuity and bonding role of the frozen phase. If a larger proportion of the pore space is occupied by liquid brine, the ice-soil skeleton becomes less continuous and the strength is reduced (Hivon and Sego, 1995). This effect has been observed previously in frozen saline soils and in coarse-grained sands, where salinity promotes the retention of highly saline unfrozen water in the pore network during freezing (Hivon and Sego, 1995; Arenson and Sego, 2006). The present study therefore interprets strength changes through the phase state of the pore fluid rather than through temperature alone.

This framework leads directly to the working hypotheses of the experimental programme. At -10 °C, which lies above the eutectic temperature of the NaCl-H_2O system, increasing NaCl concentration is expected to increase the amount of unfrozen brine and to reduce unconfined compressive strength. At -25 °C, which lies below the eutectic, residual brine is expected to solidify in a second freezing stage, so that the mechanical response should differ from that observed at -10 °C even at the same initial salt concentration. The role of the experiments is therefore to determine how strongly these thermodynamic expectations are expressed in the measured freezing curves, unfrozen water contents and strength data.

3 Methodology

3.1 Material and specimen preparation

A narrow-graded sand with particle sizes between 0.5 mm and 1.0 mm was selected for the experimental programme. The use of a coarse-grained material was intended to minimise pore-size-controlled freezing effects and thereby allow the influence of salinity to be assessed more directly (Watanabe and Mizoguchi, 2002; Arenson and Sego, 2004; Xiao, Lai and Zhang, 2018). The use of a narrow particle-size range also avoids additional variability associated with mixed soil gradations, for which the coarse-grained fraction can strongly influence the mechanical response of frozen soils (Liu et al., 2019). In any case the controlled nature of the experiments guarantees that pore size and structure are similar on all samples.

Sodium chloride (NaCl) was used as the dissolved salt. In contrast to salts that may precipitate during the early stages of cooling and alter pore structure, NaCl is suitable for investigating the thermodynamic effect of salinity in a comparatively controlled manner within the concentration range considered here (Wan et al., 2015).

Cylindrical specimens with a diameter of 50 mm and a height of 100 mm were prepared for freezing-curve measurements and unconfined compression testing. This height-to-diameter ratio of 2:1 follows established practice for frozen-soil testing (Andersland and Ladanyi, 2004). The specimens were formed in cylindrical polyurethane moulds. The mould base contained a lead-through for the installation of a temperature sensor at specimen mid-height.

The specimens were prepared under saline solution to maximise saturation and minimise entrapped air. First, the required amount of NaCl solution was poured into the mould. The sand was then placed in four layers, each of which was lightly compacted. This preparation procedure resulted in initial degrees of saturation between 0.95 and 1.0 and porosities between 0.391 and 0.413 before freezing. The NaCl concentration of the pore fluid ranged from 0.0% to 10.0% by mass of solution. Throughout this paper, NaCl concentration refers to the initial concentration of the saturating solution, expressed as mass percent NaCl by mass of solution.

After preparation, the specimens were frozen for 24 h in the controlled freezing laboratory. Each specimen was frozen once only and was not subjected to freeze-thaw cycling. The moulds were left open at the top to accommodate the volumetric expansion associated with water-ice phase change. Excess material extruded during freezing was removed after freezing to obtain uniform specimen dimensions.

The homogeneity of the preparation method was checked by cutting frozen specimens into three horizontal layers and determining porosity and water content by oven drying. The measured mean porosity was 0.411 ± 0.015, with a maximum variation over the specimen height of ± 0.024. After freezing and drying, the mean degree of saturation was 0.83. This reduction relative to the initial condition is attributed to pore-water loss during freezing as a result of volumetric expansion.

3.2 Freezing-curve measurements

The experiments were carried out in the controlled freezing laboratory of GUT, in which ambient temperatures between -4 °C and -30 °C can be maintained with an accuracy of ± 0.5 °C. Specimens remained in the laboratory throughout preparation, freezing and testing in order to avoid thermal disturbance.

A PT100 temperature sensor was installed at mid-height in each specimen used for freezing-curve measurements. Temperature was recorded at 1 s intervals during cooling. Two ambient temperatures were investigated, namely -10 °C and -25 °C. These temperatures were selected to represent conditions above and below the eutectic temperature of the NaCl-H_2O system, respectively.

The freezing curves were used to identify the initial supercooling stage, the onset of ice formation and the duration of the subsequent temperature plateau or plateaux. All freezing-curve specimens were cooled 24 hours until the specimen temperature approached the imposed ambient temperature.

3.3 Unconfined compression testing

Unconfined compression tests were performed on specimens that had been frozen for at least 24 h. This ensured that the primary freezing process had been completed before mechanical loading. The tests were conducted in the freezing laboratory under temperature-controlled conditions.

For the compression tests, additional PT100 sensors were installed at the specimen top and base, while the central sensor remained at mid-height. Before testing, a specimen was considered to be at thermal steady state when the temperature difference between top, middle and base did not exceed 0.3 °C for at least 1 h. Typical temperature gradients at failure were less than 0.5 °C over the specimen height.

The tests were performed at a constant axial strain rate of 0.1%/min and were terminated at 20% axial strain. This strain rate was selected to remain within established frozen-soil testing practice while limiting additional rate effects in specimens that were expected to contain unfrozen brine at -10 °C (Andersland and Ladanyi, 2004).

Axial deformation was measured using linear variable displacement transducers, and axial load was recorded using a 2 t load cell. For the salt-free reference specimens, which developed substantially higher strengths, a 10 t load cell was used. The linear variable displacement transducers had an accuracy better than ± 0.05 mm, and both load cells had an accuracy better than ± 0.5% of nominal load. For each test condition, three nominally identical specimens were tested.

3.4 NMR measurements of unfrozen water content

Additional measurements were performed to quantify unfrozen water content by nuclear magnetic resonance. For these tests, specimens were prepared in sealed glass tubes with an inner diameter of 27 mm and a height of 55 mm. The specimens were frozen at -10 °C. In addition, a reference NaCl solution without sand was prepared and measured under the same conditions. Unfrozen-water measurements were performed at -10 °C because this temperature lies above the eutectic and saline brine is expected to persist in the pore space. Additional

NMR measurements were not performed at -25 °C. At this temperature, the NaCl-H_2O phase diagram indicates that the system lies below the eutectic temperature, so residual brine is expected to have largely solidified under equilibrium conditions. The interpretation of the -25 °C response is therefore based on the freezing curves, the strength data and the phase-diagram framework, rather than on direct NMR measurements at that temperature.

All NMR measurements were carried out using a low-field Halbach NMR spectrometer operating at 3.91 MHz (Halbach, 1980; Anferova et al., 2007). The Carr-Purcell-Meiboom-Gill pulse sequence was used for the relaxation measurements (Carr and Purcell, 1954; Meiboom and Gill, 1958). The shortest echo time in the present set-up was 320 µs and, depending on sample response, up to 2500 echoes were recorded. Individual measurements were averaged until a signal-to-noise ratio of approximately 200 was achieved.

To position the sample within the sensitive range of the NMR device, spacers were placed beneath the sample tube before measurement. The excitation frequency was then adjusted to the operating frequency of the instrument. During measurement, cooling had to be switched off to avoid electromagnetic disturbance from the freezing unit. For this reason, the measurement sequence for each specimen consisted of a reference solution measurement, the sand specimen measurement and a second reference solution measurement, with temperature checks before and after each step. The average of the two reference measurements was used to account for minor temperature changes during the test sequence. Further details of the NMR procedure are given in Appendix **A**.

4 Experimental results

4.1 Freezing behaviour at -10 °C

Figure **2** shows the freezing curves obtained at an ambient temperature of -10 °C for specimens with different NaCl concentrations. The salt-free specimen exhibited the typical freezing response of a saturated sand specimen. After supercooling to about -0.7 °C, crystallisation started and the specimen temperature rose to a freezing plateau at about -0.1

°C, which lasted approximately 3.5 h. After this plateau, the specimen temperature decreased gradually to about -3.0 °C and then fell more rapidly towards the ambient temperature.

With increasing NaCl concentration, three systematic changes were observed. First, both the supercooling temperature and the freezing plateau temperature decreased. Second, the duration of the first temperature plateau became shorter. Third, the cooling phase after the plateau became more gradual, and specimens with higher salinity required longer to approach the ambient temperature. Appendix **B** shows a simple calculation of the plateau times using a physics-based plausible approach that supports the experimental results and can be of assistance for experimental design.

These observations indicate a progressive change in freezing behaviour with increasing salinity at -10 °C. The freezing curves show that the early freezing event becomes less pronounced and that the subsequent cooling stage extends over a longer period as NaCl concentration increases.

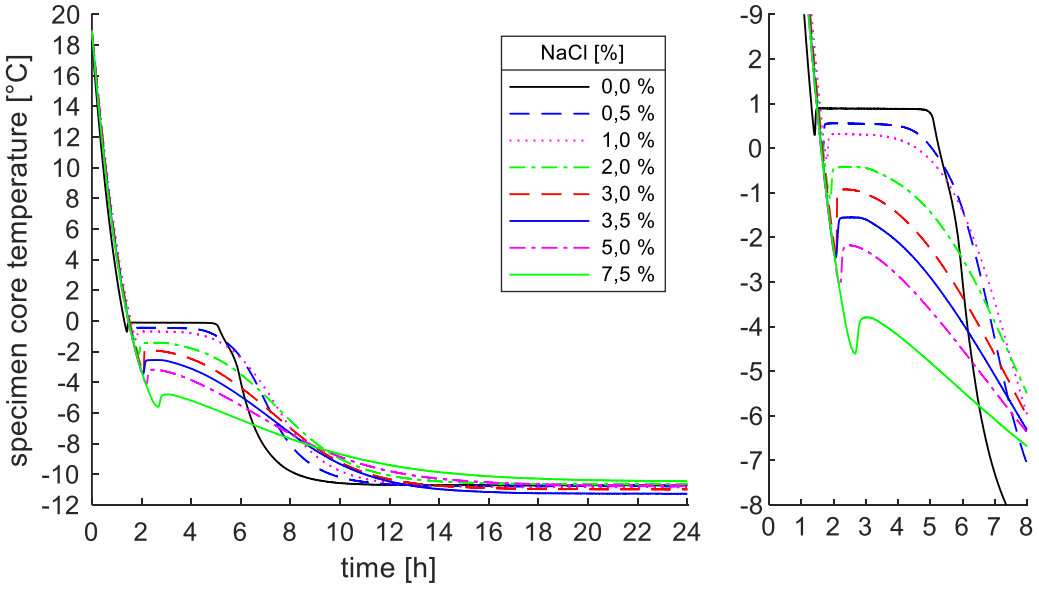

Fig. 2. Freezing curves of sand specimens with different NaCl concentrations at an ambient temperature of -10 °C. Increasing NaCl concentration lowers the supercooling and freezing temperatures, shortens the first plateau and prolongs the subsequent cooling stage.

4.2 Freezing behaviour at -25 °C

Figure **3** shows the freezing curves obtained at an ambient temperature of -25 °C. Cooling was faster than at -10 °C, and the supercooling and first freezing stages occurred earlier in time. The first temperature plateau was also shorter than for the corresponding tests at -10 °C.

For specimens containing more than 0.5% NaCl, a second temperature rise was observed after the first freezing stage, when the specimen temperature had fallen to about -23 to -24 °C. This second plateau was absent in the salt-free specimen and became increasingly pronounced with increasing NaCl concentration. Its duration increased disproportionately for concentrations above 5% NaCl. The specimens containing 7.5% and 10.0% NaCl showed the longest second plateau durations.

The freezing curves at -25 °C therefore differ qualitatively from those at -10 °C. In addition to the earlier first freezing event, a second freezing stage was recorded in the saline specimens.

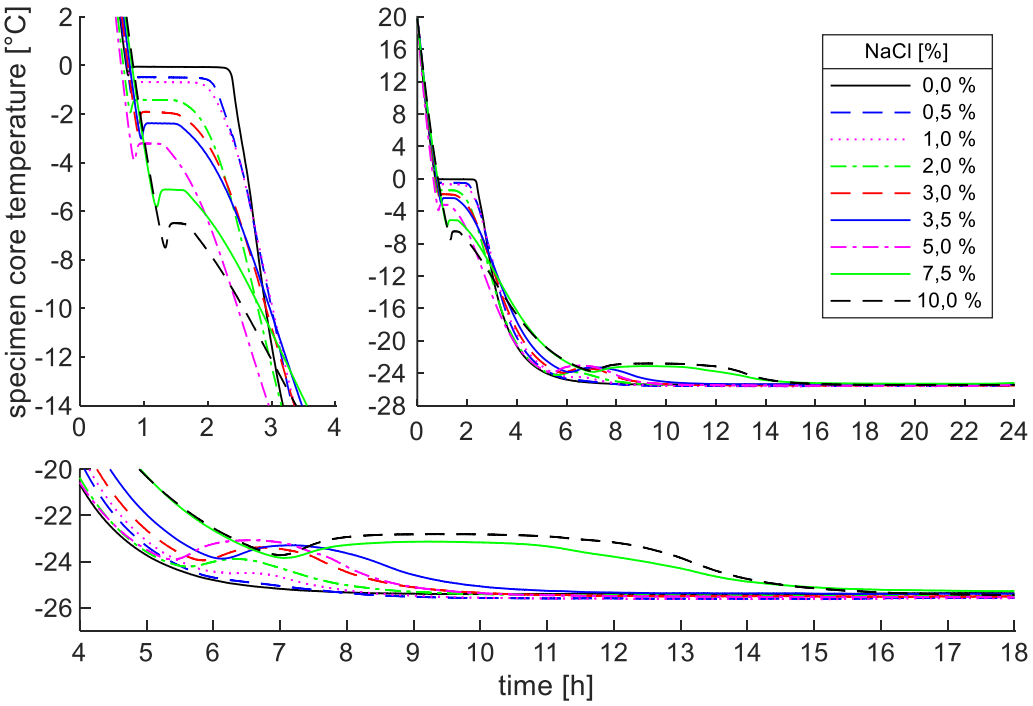

Fig. 3. Freezing curves of saturated sand specimens with different initial NaCl concentrations at an ambient temperature of -25 °C. Saline specimens exhibit a second temperature plateau at approximately -23 to -24 °C, interpreted as a eutectic freezing stage of residual brine.

4.3 Unconfined compressive strength

The measured peak stresses are summarised in Figure **4a**, and the same data normalised to the corresponding salt-free reference values are shown in Figure **4b**. Each point represents one test. Three specimens were tested for each condition.

At -10 °C, unconfined compression tests were performed for NaCl concentrations up to 7.5%. Higher concentrations could not be tested because the specimens had insufficient strength. The repeatability of the measurements was good. The ratio of standard deviation to mean value was below 6.0% up to 5.0% NaCl and 9.1% at 7.5% NaCl.

The peak stress decreased strongly with increasing NaCl concentration at -10 °C. The largest reduction occurred at very low salinity. At 0.5% NaCl, the peak stress was already reduced to about 25% of the salt-free reference value. Beyond this point, the reduction in peak stress with increasing salinity was approximately linear, although local deviations were observed.

At -25 °C, peak stresses were substantially higher than at -10 °C for the corresponding NaCl concentrations. The repeatability of these tests was also high. The ratio of standard deviation to mean value was below 1.3% for all saline specimens, 2.5% at 0.75% NaCl and 3.4% for the salt-free reference specimen.

The strength trend at -25 °C was not monotonic. From 0.0% to about 0.25% NaCl, peak stress decreased. Between about 0.25% and 1.0% NaCl, the strength showed a partial recovery or plateau. At higher NaCl concentrations, the peak stress decreased again. After normalisation to the salt-free reference value, the maximum observed reduction at -25 °C was about 50%, which was substantially smaller than the reduction already observed at 0.5% NaCl at -10 °C.

4.4 Unfrozen water content from NMR and phase-diagram-based estimate of unfrozen water fraction

The NMR results obtained at -10 °C are shown in Figure **4b** and summarised in Table **2**. The fraction of unfrozen water increased almost linearly with NaCl concentration. At 10.0% NaCl, approximately 78.3% of the pore water remained liquid, leaving only about 21.7% in the frozen phase.

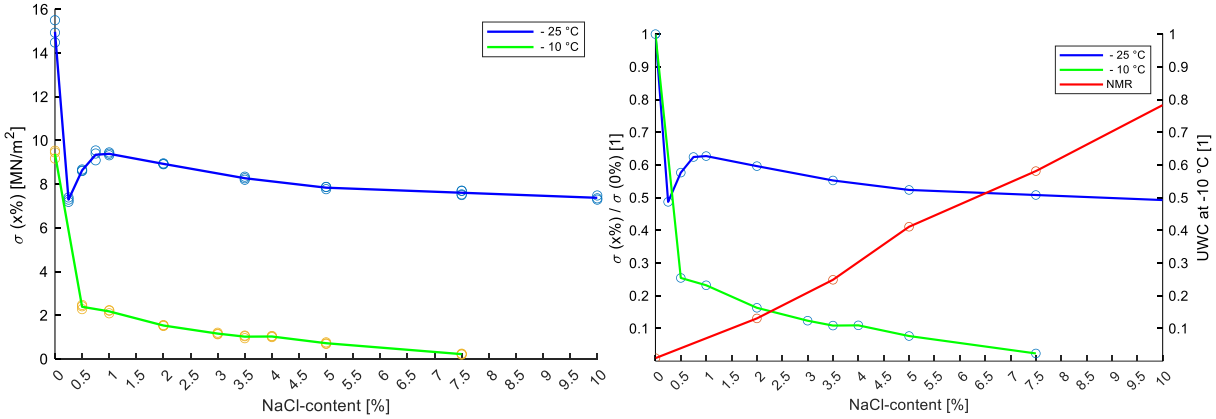

Fig. 4. Influence of initial NaCl concentration on mechanical and phase response of frozen sand: (a) peak unconfined compressive strength at -10 °C and -25 °C. Each strength point represents one UCS test; (b) peak strength normalised by the corresponding salt-free reference value, together with the unfrozen liquid fraction measured by NMR at -10 °C. Each strength point represents the mean value of the UCS test series.

For the salt-free specimen, the measured unfrozen water fraction was about 0.91%. With increasing NaCl concentration, the measured unfrozen water fraction increased to 13.06% at 2.0% NaCl, 24.87% at 3.5% NaCl, 58.11% at 7.5% NaCl and 78.29% at 10.0% NaCl.

Taken together, Figure **4** shows that the increase in unfrozen water fraction at -10 °C is accompanied by a strong reduction in compressive strength, while the normalised strength response differs markedly between -10 °C and -25 °C.

We then tested the ability of the lever rule applied to the phase diagram with an idealised thermodynamic estimate, to predict the liquid fraction of the NaCl-H_2O system at -10 °C. This was compared to the NMR measurements. For a given bulk NaCl concentration C_0, the theoretical liquid (brine) fraction $f_{\text{liq, ideal}}$ in the two-phase field was estimated as:

$$f_{\text{liq, ideal}}(C,T) = \frac{C - C_{\text{sol}}(T)}{C_{\text{liq}}(T) - C_{\text{sol}}(T)} \quad (1)$$

where

- C is the bulk *NaCl* concentration,
- $C_{\text{sol}}(T)$ is the solid concentration (ice boundary),
- $C_{\text{liq}}(T)$ is the liquid concentration (brine boundary).

However, even salt-free specimens retain a small liquid fraction due to pore-scale forces (e.g. van der Waals interactions). NMR tests on the 0% NaCl sample indicated ~1% residual liquid water. To account for this, the corrected liquid fraction is expressed below and is used for the comparisons in Table **2**.

$$f_{\text{liq}}(C,T) = f_{\text{liq, ideal}}(C,T) + 0.01 \quad (2)$$

The lever-rule calculation is intended as a first-order phase-diagram-based estimate of unfrozen water fraction, but it yet provides reasonable results. The errors may stem from pore-scale curvature effects, salt redistribution during freezing or local deviations from equilibrium that are not considered in the approach.

Table 2. Measured unfrozen water fraction at -10 °C from NMR and corresponding corrected lever-rule estimate for different NaCl concentrations.

$\%\ NaCl$	$f_{\text{liq, ideal}}(C,T)$	$f_{\text{liq}}(C,T)$	***NMR results***	***Relative error*** $RE = \frac{\lvert f_{\text{liq}}(C,T) - NMR \rvert}{\lvert NMR \rvert} * 100\%$
0.5	0.033	0.043	-	-
1.0	0.067	0.077	-	-
2.0	0.133	0.143	0.131	9.16
3.5	0.233	0.243	0.249	2.41
5.0	0.333	0.343	0.411	16,55
7.5	0.500	0.510	0.581	12,22
10.0	0.667	0.677	0.783	13.54

5 Discussion

5.1 Phase-diagram interpretation of the freezing curves

The freezing curves can be interpreted consistently within the framework of the NaCl-H_2O phase diagram introduced in Section **2**. At -10 °C, all saline specimens remained above the eutectic temperature of the system. Under these conditions, freezing proceeds by preferential crystallisation of relatively pure ice, while the remaining liquid becomes progressively enriched in NaCl (Banin and Anderson, 1974; Atkins, 1996). The observed reduction in freezing temperature with increasing salinity is therefore consistent with the thermodynamic effect of dissolved salt on the liquid phase. The shortening of the first plateau with increasing NaCl concentration further indicates that a smaller fraction of the pore water solidified during the initial freezing stage.

At -25 °C, the freezing response changed qualitatively. In addition to the first freezing stage, saline specimens exhibited a second plateau once the specimen temperature had fallen to about -23 to -24 °C. This second stage is consistent with the approach to eutectic conditions and the subsequent solidification of the remaining brine (Journaux et al., 2023). Its absence in the salt-free specimens and its increasing duration with increasing NaCl concentration support this interpretation. The freezing curves therefore show that the governing phase state differs fundamentally between the two test temperatures: at -10 °C, the pore space contains ice and saline unfrozen water, whereas at -25 °C the cooling path extends below the eutectic and residual brine is no longer expected to remain liquid in significant quantities.

The comparison between measured unfrozen water contents and the corrected lever-rule estimate supports this phase-diagram-based interpretation of the freezing curves. At -10 °C, agreement was close up to salinities below 5.0% NaCl, indicating that the first-order phase behaviour of the system is captured well by the NaCl-H_2O framework. At higher concentrations, the measured unfrozen water fraction exceeded the idealised estimate. This deviation is most plausibly attributed to processes not represented in the lever-rule approach, including pore-scale interfacial effects, local salt redistribution during freezing and departures from ideal

358 equilibrium in the soil pore network (Watanabe and Mizoguchi, 2002; Zhou et al., 2018; Luo et
359 al., 2023).

360 **5.2 Linking salinity, unfrozen water and strength**

361 Because unfrozen-water content was measured directly only at -10 °C, the interpretation of the
362 -25 °C response is based on the freezing curves, strength data, and the NaCl-H_2O phase
363 diagram. The combined freezing-curve, NMR and strength data show that salinity influences
364 frozen-soil behaviour not only through freezing point depression, but through a coupled change
365 in phase state and mechanical response. The clearest result is the large strength loss observed
366 at -10 °C. At this temperature, even 0.5% NaCl reduced the peak strength to about one quarter
367 of the salt-free reference value. This finding is consistent with the general understanding that
368 frozen-soil strength decreases as the amount of unfrozen water increases and the continuity
369 of the ice skeleton is reduced (Hivon and Sego, 1995; Watanabe and Mizoguchi, 2002).
370 However, the present data show that the reduction in strength is more nonlinear than the
371 increase in unfrozen water fraction alone.

372 This distinction is important. The NMR data indicate an almost linear increase in unfrozen water
373 fraction with increasing NaCl concentration at -10 °C, whereas the relative strength loss is
374 steepest at low salinities and becomes less steep over the intermediate range. This suggests
375 that the first increase in unfrozen brine has a particularly strong effect on the continuity of the
376 load-bearing ice-soil skeleton. In other words, the relationship between unfrozen water and
377 strength is not purely volumetric. The data are consistent with the interpretation that small
378 amounts of saline unfrozen water disproportionately disrupt ice bonding and reduce the
379 mechanical effectiveness of the frozen matrix. This interpretation is also in line with earlier
380 observations that salinity can promote the retention of highly saline unfrozen water within the
381 pore structure of coarse-grained frozen soils (Arenson and Sego, 2004; Arenson and Sego,
382 2006), and with recent evidence that frozen saline sand may retain connected liquid pathways
383 even under frozen conditions (Gao et al., 2024).

384 The behaviour at -25 °C is different. Once the specimens are cooled below the eutectic
385 temperature, the residual brine undergoes a second freezing stage and the strength response

no longer follows the same pattern as at -10 °C. The strength does not decrease monotonically with NaCl concentration over the full range investigated. Instead, a local plateau or partial recovery is observed between about 0.25% and 1.0% NaCl before strength decreases again at higher salinities. The most robust conclusion is therefore that cooling below the eutectic temperature changes the dominant factors controlling the observed mechanical response. At -25 °C, the strength response cannot be interpreted solely in terms of persistent liquid brine in the same way as at -10 °C. Instead, the frozen matrix contains the solid products of eutectic freezing, so the saline frozen soil is mechanically different from both unfrozen brine-bearing soil and salt-free frozen soil.

The non-monotonic strength response observed at -25 °C can be interpreted qualitatively from the change in phase assemblage across the eutectic. At -10 °C, the NaCl-H2O system lies above the eutectic and the pore space contains ice and saline unfrozen brine, so strength is reduced by the persistence of liquid within the frozen skeleton. At -25 °C, by contrast, the system passes below the eutectic and the remaining brine is expected to solidify; at 1 bar, the relevant solid assemblage near this temperature is ice Ih plus hydrohalite (NaCl·2H2O) rather than liquid brine (Journaux et al., 2023; Bartels-Rausch et al., 2021). This phase change provides a plausible explanation for the qualitative change in strength behaviour and for the partial recovery relative to the above-eutectic condition. However, the phase diagram alone cannot explain the exact local plateau in strength at low salinity, because it does not constrain the spatial distribution, connectivity or bonding role of the newly formed solid phases within the pore network. The detailed microstructural origin of this non-linearity therefore remains to be verified experimentally.

5.3 Comparison to empirical relationships in the literature

For comparison, the measured strength–unfrozen-water relationship was evaluated against empirical relationships proposed in the literature. The purpose of this comparison is not to propose a general constitutive model, but to assess whether existing empirical forms can reproduce the nonlinear strength reduction observed in the present dataset.

In particular, we use the power law presented by Ren et al. (2023) and the exponential fitting curve suggested by Li et al. (2025). Ren et al (2023) proposed $\boldsymbol{\sigma(UWC) = \sigma_0 * UWC^m}$ and Li et al (2025) proposed an exponential relationship that we have modified by adding a correction of the UWC_0 from the reference sample, $\boldsymbol{\sigma(UWC) = \sigma_0 * e^{-c*(UWC-UWC_0)}}$, where *m* and *c* are model coefficients. Fig. **5** shows the results of the fit to our data and the goodness of the fit, expressed as R^2. Fitted values of $\boldsymbol{\sigma_0 = 9.38\ MN/m^2}$, $\boldsymbol{UWC_0 = 0.91\ \%}$ **and *m* = -0.706** were used for Ren's model. Two options for Li et al are presented. One for a constant value of ***c* = 0.095**, and one where *c* is calculated using a fitted second order polynomial as a function of UWC content (see Appendix **C**). The latter shows a clearly better result.

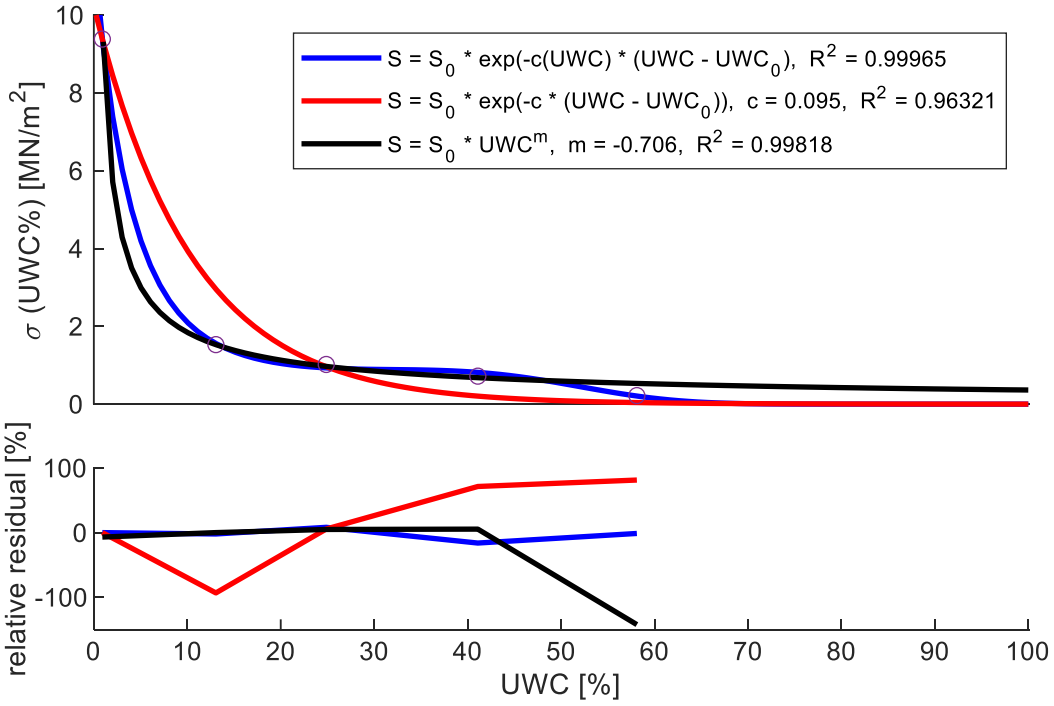

Fig. 5. Soil strength over UWC. The dots show the experimental results. Various models for fitting the test results are shown, along with the relative residual error $e = \frac{y-\bar{y}}{y} * 100\%$ where y describes the measured value and $\bar{y}$ the value proposed by the model.

The fitted curves support the interpretation drawn from the experimental observations: the mechanical effect of salinity is controlled not only by how much liquid remains in the pore space, but by how that liquid disrupts the continuity and effectiveness of the frozen skeleton. Salt introduces a second-order effect that cannot be captured by the existing relationships. Both

curves from the literature are though incapable of reproducing the results shown for -25 °C. Our second-order polynomial approach fits the data much better. Although not intended as a universal estimation curve, it identifies a clear gap and highlights the importance of the experimental results presented here.

6 Conclusions

This study examined the influence of NaCl on the freezing behaviour, unfrozen water content and unconfined compressive strength of fully saturated, narrow-graded sand at -10 °C and -25 °C. By combining freezing curves, NMR measurements and mechanical tests, the study provides a controlled thermo-mechanical dataset that links phase behaviour, unfrozen water and strength in saline frozen sand.

The main conclusions are as follows.

- Increasing NaCl concentration systematically lowered both the supercooling temperature and the freezing temperature of the specimens. The measured freezing curves were consistent with the NaCl-H_2O phase framework and showed that, at -10 °C, a significant fraction of saline pore fluid remained unfrozen.
- At -25 °C, saline specimens exhibited a second plateau in the freezing curves, consistent with eutectic solidification of residual brine. The corresponding strength response was non-monotonic, with a local plateau or partial recovery at low salinity before strength decreased again at higher NaCl contents. This indicates that below-eutectic behaviour cannot be interpreted simply as a colder extension of the above-eutectic response.
- Salinity had a pronounced effect on mechanical behaviour. At -10 °C, even a small NaCl addition caused a disproportionate loss of strength at low salt concentrations. In particular, 0.5% NaCl reduced the peak strength to about one quarter of the salt-free reference value. This shows that low salinity can strongly weaken frozen sand even when the material is already below 0 °C.

- The NMR measurements at -10 °C showed an almost linear increase in unfrozen water content with increasing NaCl concentration. The comparison with the corrected lever-rule estimate showed good agreement to salinities below 5.0% NaCl, while larger deviations at higher concentrations indicate additional pore-scale effects and salt redistribution during freezing.
- The relationship between unfrozen water content and strength was strongly nonlinear. The first increase in unfrozen water content produced the largest relative loss of strength, indicating that the mechanical response is controlled not only by the amount of liquid phase present, but also by its effect on the continuity and effectiveness of the frozen soil skeleton.
- Below the eutectic, the strength response changed qualitatively. At -25 °C, a local plateau or partial recovery in strength was observed at low salinity before strength decreased again at higher NaCl contents. This indicates that once residual brine solidifies, the mechanical response of saline frozen sand differs from that observed above the eutectic and cannot be interpreted simply as a colder version of the salt-free case.
- The empirical strength–unfrozen-water fits provide a useful description of the present dataset, but should not be interpreted as general constitutive relationships. Their main value is to show that existing simple relationships do not fully capture the coupled effects of salinity, unfrozen water fraction and below-eutectic phase change.

From an engineering perspective, the results show that salinity must be treated as a primary design variable in frozen ground. Above the eutectic, even low NaCl contents can severely reduce strength because unfrozen brine remains in the pore space. Below the eutectic, a second freezing stage occurs and the governing mechanical response changes. For artificial ground freezing and saline frozen ground, both the thermal and mechanical consequences of salinity therefore need to be considered explicitly.

The results are limited to nearly fully saturated, narrow-graded sand with NaCl pore fluid, tested at two temperatures and under one loading condition. They should therefore not be transferred

directly to fine-grained soils, other salts, partial saturation or different loading paths without further investigation. Even so, the present study provides a clear experimental basis for understanding how salinity alters the coupled thermal and mechanical behaviour of frozen sand.

Acknowledgements

We sincerely thank the laboratory team of GUT for their excellent and reliable assistance. Special thanks to Prof. Dr. Norbert Klitzsch of the Institute for Applied Geophysics and Geothermal Energy to enable the use of their NMR device at the E.ON ERC laboratory.

Funding

This work was supported by the Deutsche Forschungsgemeinschaft (DFG, German Research Foundation) [grant number 505704399].

Data statement

Data supporting this study are available upon request.

References

Amankwah, S.K., Ireson, A.M., Maulé, C., Brannen, R., Mathias, S.A., 2021. A model for the soil freezing characteristic curve that represents the dominant role of salt exclusion. Water Resources Research, 57(8), e2021WR030070. https://doi.org/10.1029/2021WR030070

Andersland, O.B., Ladanyi, B., 2004. Frozen ground engineering. John Wiley & Sons.

Anderson, D.M., Tice, A.R., 1972. Predicting unfrozen water contents in frozen soils from surface area measurements. Highway research record, 393(2), 12-18.

Anderson, D.M., Tice, A.R., 1973. The unfrozen interfacial phase in frozen soil water systems. In Physical aspects of soil water and salts in ecosystems (pp. 107-124).

Berlin, Heidelberg: Springer Berlin Heidelberg. https://doi.org/10.1007/978-3-642-65523-4_12

Anferova, S., Anferov, V., Arnold, J., Talnishnikh, E., Voda, M.A., Kupferschläger, K., ..., Blümich, B., 2007. Improved Halbach sensor for NMR scanning of drill cores. Magnetic resonance imaging, 25(4), 474-480. https://doi.org/10.1016/j.mri.2006.11.016

Arenson, L.U., Sego, D.C., 2004. Freezing processes for a coarse sand with varying salinities. In Proceedings of the Cold Regions Engineering & Construction Conference, Edmonton, Alta (Vol. 16719).

Arenson, L.U., Sego, D.C., 2006. The effect of salinity on the freezing of coarse-grained sands. Canadian Geotechnical Journal, 43(3), 325-337. https://doi.org/10.1139/t06-006

Atkins, P.W., 1996. Physikalische Chemie, 2. Auflage. VCH.

Banin, A., Anderson, D.M., 1974. Effects of salt concentration changes during freezing on the unfrozen water content of porous materials. Water Resources Research, 10(1), 124-128. https://doi.org/10.1029/WR010i001p00124

Bartels-Rausch, T., Kong, X., Orlando, F., Artiglia, L., Waldner, A., Huthwelker, T., Ammann, M., 2021. Interfacial supercooling and the precipitation of hydrohalite in frozen NaCl solutions as seen by X-ray absorption spectroscopy, The Cryosphere, 15, 2001–2020. https://doi.org/10.5194/tc-15-2001-2021

Carr, H.Y., Purcell, E.M., 1954. Effects of diffusion on free precession in nuclear magnetic resonance experiments. Physical review, 94(3), 630-638. https://doi.org/10.1103/PhysRev.94.630

Gao, X., Tian, R., Jiang, Y., Guo, Z., Lei, L., 2024. Frozen saline sand can be highly permeable. Geophysical Research Letters, 51(19), e2024GL111946. https://doi.org/10.1029/2024GL111946

Haghighi, H., Chapoy, A., Tohidi, B., 2008. Freezing point depression of electrolyte solutions: experimental measurements and modeling using the cubic-plus-association equation

of state. Industrial & engineering chemistry research, 47(11), 3983-3989. https://doi.org/10.1021/ie800017e

Halbach, K., 1980. Design of permanent multipole magnets with oriented rare earth cobalt material. Nuclear instruments and methods, 169(1), 1-10. https://doi.org/10.1016/0029-554X(80)90094-4

Hivon, E.G., Sego, D.C., 1995. Strength of frozen saline soils. Canadian Geotechnical Journal, 32(2), 336-354. https://doi.org/10.1139/t95-034

Jessberger, H., Jagow-Klaff, R., 2001. Bodenvereisung. Grundbau-Taschenbuch, Teil 2: Geotechnische Verfahren, S. 121-166.

Journaux, B., Pakhomova, A., Collings, I.E., Petitgirard, S., Boffa Ballaran, T., Brown, J.M., ..., Hanfland, M., 2023. On the identification of hyperhydrated sodium chloride hydrates, stable at icy moon conditions. Proceedings of the National Academy of Sciences, 120(9), e2217125120. https://doi.org/10.1073/pnas.2217125120

Ju, Z., Lu, S., Guo, K., Liu, X., 2023. Changes in the thermal conductivity of soil with different salts. Journal of Soils and Sediments, 23(9), 3376-3383. https://doi.org/10.1007/s11368-023-03564-1

Li, X., Li, X., Liu, J., 2024. A dynamic soil freezing characteristic curve model for frozen soil. Journal of Rock Mechanics and Geotechnical Engineering, 16(8), 3339-3352. https://doi.org/10.1016/j.jrmge.2023.09.008

Li, Z., Yang, G., Wang, B., Wang, J., 2025. Study on unfrostered water content and strength characteristics of saturated sandstone during thawing process. Scientific Reports, 15(1), 17641. https://doi.org/10.1038/s41598-025-01558-2

Liu, X., Liu, E., Zhang, D., Zhang, G., Yin, X., Song, B., 2019. Study on effect of coarse-grained content on the mechanical properties of frozen mixed soils. Cold Regions Science and Technology, 158, 237-251. https://doi.org/10.1016/j.coldregions.2018.09.001

Loomis, E.H., 1896. On the freezing-points of dilute aqueous solutions. Physical Review (Series I), 3(4), 270. https://doi.org/10.1103/PhysRevSeriesI.3.270

564 Luo, C.L., Yu, Y.Y., Zhang, J., Tao, J.Y., Ou, Q.J., Cui, W.H., 2023. Thermal-water-salt
565 coupling process of unsaturated saline soil under unidirectional freezing. Journal of
566 Mountain Science, 20(2), 557-569. https://doi.org/10.1007/s11629-022-7652-7
567 McKenzie, J.M., Voss, C.I., Siegel, D.I., 2007. Groundwater flow with energy transport and
568 water–ice phase change: Numerical simulations, benchmarks, and application to
569 freezing in peat bogs. Advances in water resources, 30(4), 966-983.
570 https://doi.org/10.1016/j.advwatres.2006.08.008
571 Meiboom, S., Gill, D., 1958. Modified spin-echo method for measuring nuclear relaxation
572 times. Review of Scientific Instruments, 29(8), 688. https://doi.org/10.1063/1.1716296
573 Mitchell, J., Webber, J.B.W., Strange, J.H., 2008. Nuclear magnetic resonance
574 cryoporometry. Physics Reports, 461(1), 1-36.
575 https://doi.org/10.1016/j.physrep.2008.02.001
576 Orth, W., Solf, O., Perl, C., Rizos, D., 2021. STUVA Conference 2021, Karlsruhe. ISBN 978-
577 3-00-070615-8.
578 Ren, Z., Liu, J., Jiang, H., Wang, E., 2023. Experimental study and simulation for unfrozen
579 water and compressive strength of frozen soil based on artificial freezing technology.
580 Cold Regions Science and Technology, 205, 103711.
581 https://doi.org/10.1016/j.coldregions.2022.103711
582 Rizos, D., Orth, W., Perl, C., Solf, O., Eramo, N., Amin, T., 2022. Port Said Tunnels under
583 the Suez Canal - Cross passages with ground freezing in aggressive conditions. In
584 Proceedings of the World Tunnel Congress (WTC). Copenhagen: ITA Bookshop.
585 ISBN 978-2-9701436-7-3
586 Wan, X., Lai, Y., Wang, C., 2015. Experimental study on the freezing temperatures of saline
587 silty soils. Permafrost and Periglacial Processes, 26(2), 175-187.
588 https://doi.org/10.1002/ppp.1837
589 Wan, X., Liu, E., Qiu, E., 2021. Study on ice nucleation temperature and water freezing in
590 saline soils. Permafrost and Periglacial Processes, 32(1), 119-138.
591 https://doi.org/10.1002/ppp.2081

592 Wan, X., Zhu, J., Lai, Y., Lu, J., Yan, Z., 2024. Premelting theory-based mechanism for water
593 freezing in saline soil. Water Resources Research, 60(10), e2024WR038013.
594 https://doi.org/10.1029/2024WR038013
595 Wang, C., Li, K., Cai, H., Wu, Y., Lin, Z., Li, S., 2023. Study of Supercooling Phenomena in
596 Soil-Water Systems Based on Nucleation Theory: Quantifying Supercooling Degree.
597 Water Resources Research, 59(11), e2023WR035935.
598 https://doi.org/10.1029/2023WR035935
599 Watanabe, K., Mizoguchi, M., 2002. Amount of unfrozen water in frozen porous media
600 saturated with solution. Cold Regions Science and Technology, 34(2), 103-110.
601 https://doi.org/10.1016/S0165-232X(01)00063-5
602 Xiao, Z., Lai, Y., Zhang, M., 2018. Study on the freezing temperature of saline soil. Acta
603 Geotechnica, 13, 195-205. https://doi.org/10.1007/s11440-017-0537-1
604 Ying, S., Cao, Y., Zhang, Q., Xia, X., Li, G., Zhou, F., Wen, T., 2025. The effect of salt on the
605 freezing temperature of saline soil. Soils and Foundations, 65(1), 101566.
606 https://doi.org/10.1016/j.sandf.2024.101566
607 Zhou, J., Wei, C., Lai, Y., Wei, H., Tian, H., 2018. Application of the generalized Clapeyron
608 equation to freezing point depression and unfrozen water content. Water Resources
609 Research, 54(11), 9412-9431. https://doi.org/10.1029/2018WR023221

APPENDIX A - NMR measurements

For measurement purposes, samples with an inner diameter of 2.7 cm (outer diameter 3.0 cm) and a height of 5.5 cm were prepared in sealed glass tubes as recommended by Mitchell et al. (2008). This maintained a ratio of 1:2 again. Subsequently, the samples were frozen at -10 °C. A saturated NaCl solution without sand was also prepared to serve as a reference during measurement.

To carry out NMR measurements first, washers had to be placed in the NMR device to bring the sample to the correct height. The NMR device has a sensitive measuring range between heights of 70 mm and 100 mm and a highly sensitive range between 80 mm and 90 mm. Since the sample had a height of 55 mm, it was raised by adding spacers up to 60 mm beneath it. Thus, the centre of the sample lay within the sensitive measuring range. Subsequently, fine-tuning of excitation frequency was performed since it should have a value of 3.91 MHz for accurate measurement results

The measurement process for a sample proceeded as follows:

1. Measure temperature
2. NMR measurement of reference sample NaCl without sand
3. Measure temperature
4. NMR measurement of sand sample
5. Measure temperature
6. NMR measurement of reference sample NaCl without sand
7. Measure temperature

Temperature measurements between NMR measurements were necessary because during NMR measurements, cooling had to be switched off. Otherwise, electrical frequencies emitted by the freezer would disturb measurements. Each measurement took approximately half an hour during which time temperatures in the freezer increased by up to a maximum of 0.9 °C during measurement periods.

To obtain meaningful reference measurements, averages from reference measurements before and after measuring sediment samples were calculated so that any temperature difference occurring during these measurements could be corrected.

APPENDIX B - Simple 1D verification on freezing curves

A simple one-dimensional heat-transfer estimate confirms that the observed plateau durations are physically consistent and provides a simple means for prediction. The specimens (Ø 50 mm × 100 mm) had a volume of 1.96 x 10^{-4} m^3 and a surface area of 1.96 x 10^{-2} giving a characteristic length of ~0.01 m. The associated sensible-cooling time constant is 0.9–1.8 h, consistent with the non-plateau portions of the curves.

Plateau durations are then governed by latent heat release:

$$t_L = \frac{m_w L \, \Delta\theta_i(T,S)}{hA \, \Delta T_{\text{eff}}}, \tag{B.1}$$

where m_w is the specimen water mass, L the latent heat of fusion, and $\Delta\theta_i(T,S)$ the ice fraction formed at temperature T and salinity S. The ice fraction was taken from the NMR-measured liquid water contents. At –10 °C, liquid fractions increased nearly linearly with salinity, from ~0.05 (0% *NaCl*) to ~0.80 (10% *NaCl*). Using $m_w = 0.069$ kg, $L = 333.7$kJ kg^{-1}, $A = 0.0196$m², $\Delta T_{\text{eff}} \approx 10$K and two different convective coefficients: one for no salt, $h_{Sand,Water} = 9.0$ W m^{-2} K^{-1}, and one for the salty soils of $h_{Sand,Brine} = 35.0$ W m^{-2} K^{-1}, the predicted plateau durations agree well with the freezing curves (Table **B.1**). These convective coefficients are back-calculated and represent two effective overall surface coefficients. This is an oversimplification. However, the fact that a single coefficient provides a good estimate for all salty cases supports this lumped approach as a rough estimate. Additionally, with a thermal conductivity of frozen sand $k \approx 1.7$ W m^{-1}K^{-1}and the above convective coefficients (Incropera et al., 2007), the Biot number is ≪ 0.1 for the lower coefficient justifying a lumped-capacity approach, although it is only marginal for the brine.

At -25 °C, the first freezing stage is accelerated by the larger temperature gradient, but a second plateau appears near -21 °C due to eutectic freezing of residual brine. This can be described by the same expression, with $\Delta\theta_i$ representing the remaining brine fraction and ΔT_{eff} reduced to 3-5 °C. The disproportionate lengthening of this second plateau at salinities above

5% can therefore be indicated by the greater brine volume and the smaller driving temperature difference near the eutectic.

Table B.1. Predicted vs. observed plateau durations at -10 °C.

***NaCl* content [% by mass]**	**Liquid pore water from NMR [% by vol]**	**Predicted plateau duration [h]**	**Observed plateau duration [h]**
0.0	0.91	3.59	~3.5
2.0	13.06	0.81	~0.8
3.5	24.87	0.70	~0.7
7.5	58.11	0.39	~0.4
10.0	78.29	0.20	~0.2

APPENDIX C - Polynomial approximation of exponential constant *c* to UWC

To obtain a better fit of the exponential function with the experimental results, the c value at the exponent is no longer a static factor, it depends on the UWC. A second order polynomial function helps the best to take the changing influence of UWC into account. As we already know the highest impact of UWC occurs at small amounts and gets less until it´s lowest impact at around 47%. With a further rising of UWC the impact on the peak stress rises again. This follows clearly a 2nd order polynomial function.

We calculated from the exponential relation the exponent c for each experiment $\boldsymbol{\sigma(UWC) = \sigma_0 * e^{-c*(UWC-UWC_0)} \Leftrightarrow c = -\frac{ln(\sigma/\sigma_0)}{UWC-UWC_0}}$ and fit afterwards a 2nd order polynomial function (Eq. C.1) that can be seen at Figure **C.1**:

$$c(UWC) = 0.000076 * UWC^2 - 0.007233 * UWC + 0.229058 \qquad \text{(C.1)}$$

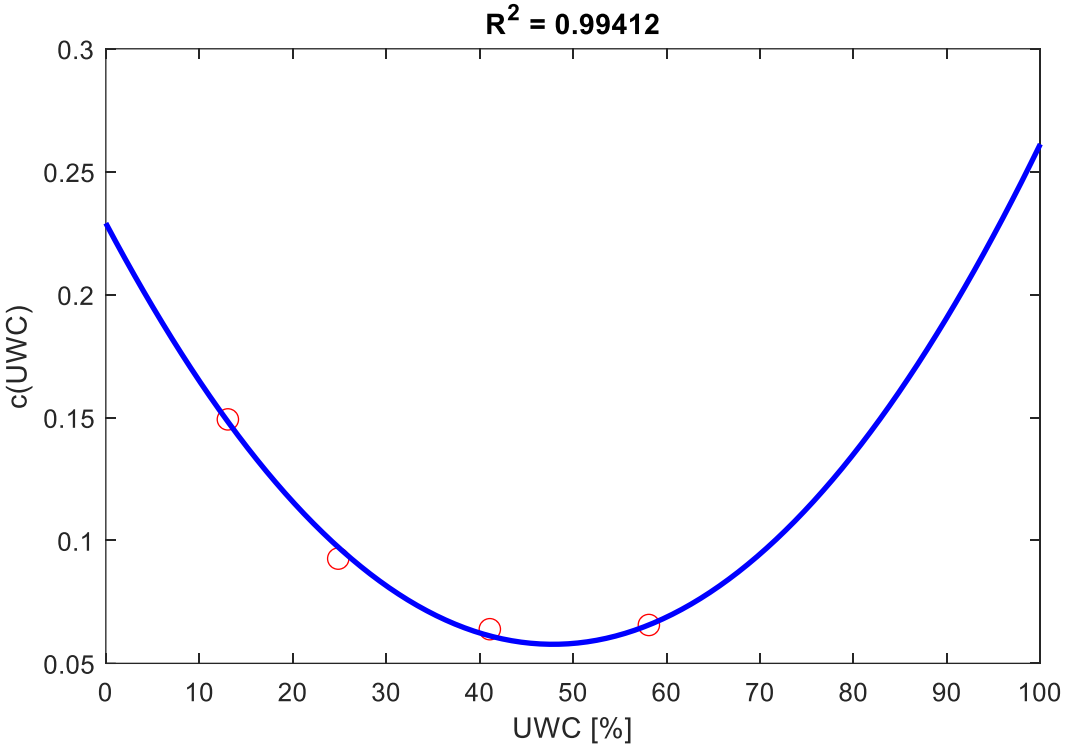

Fig. C.1. Polynomial approximation of exponential constant c to UWC.